Eur. Phys. J. E **13**, 391–400 (2004)
DOI 10.1140/epje/i2003-10085-7

THE EUROPEAN PHYSICAL JOURNAL E

Inter-lamellar interactions modulated by addition of guest components

M. Imai[1,a], R. Mawatari[1], K. Nakaya[1], and S. Komura[2]

[1] Department of Physics, Faculty of Science, Ochanomizu University, 2-1-1 Otsuka, Bunkyo, Tokyo 112-0012, Japan
[2] Department of Chemistry, Faculty of Science, Tokyo Metropolitan University, 1-1 Minami-Osawa, Hachioji, Tokyo 192-0397, Japan

Received 9 September 2003 and Received in final form 26 March 2004 /
Published online: 4 May 2004 –

Abstract. We have investigated the effects of a guest component (polymer or spherical colloidal particle) confined between flexible lamellar slits on the inter-lamellar interaction by means of a small-angle X-ray scattering technique and a neutron spin echo technique. The dominant interaction between flexible lamellar membranes without guest components is the Helfrich mechanism. The addition of a neutral polymer into the lamellar phase induces an attractive inter-lamellar interaction and finally destabilizes the lamellar phase. On the other hand, spherical colloidal particles confined between flexible lamellar membranes reduce the undulational fluctuations of lamellae and bring a repulsive inter-lamellar interaction. The behavior of the layer compression modulus of the lamellar membrane containing colloidal particles is well described by the entropical repulsive inter-lamellar interaction driven by steric hindrance.

PACS. 82.70.Uv Surfactants, micellar solutions, vesicles, lamellae, amphiphilic systems, (hydrophilic and hydrophobic interactions) – 61.25.Hq Macromolecular and polymer solutions; polymer melts; swelling – 83.80.Hj Suspensions, dispersions, pastes, slurries, colloids – 89.75.Fb Structures and organization in complex systems

1 Introduction

Complex systems consisting of surfactant membranes and guest components such as polymers or colloidal particles are widely recognized in the fields of biological membranes, drug carrier systems, lubricants, cosmetic, etc. and have acquired great interest from the scientific and industrial points of view. These systems show a characteristic phase behavior as a result of the modification of the inter-membrane interaction induced by the guest components. The lamellar phase consisting of stacks of surfactant bilayers separated by solvent layers is a suitable system to investigate the inter-membrane interaction induced by the guest components, since behaviors of the inter-lamellar interactions are well characterized by recent theoretical and experimental studies [1–4]. In this context, there are extensive studies on the ternary systems of surfactant, water, and polymers [5–17].

The role of added polymers between the lamellar bilayers was investigated theoretically by Daoud and de Gennes [5] and revisited by Brooks and Cates [7]. They classified the situations of the polymer confinement into the following four regimes and derived the corresponding free energy for each regime: 1) three-dimensional dilute solution of polymer chains (3D D), 2) three-dimensional semi-dilute solution of polymer chains (3D S-D), 3) two-dimensional semi-dilute solution of polymer chains (2D S-D) and 4) two-dimensional dilute solution of polymer chains (2D D). On the basis of these theoretical works, Ligoure *et al.* [11–13,15,16] have investigated the lyotropic lamellar system of cetyl pyridium chloride (CPCL)/hexanol/water in which a non-adsorbing water-soluble polymer polyvinylpyrolidone (PVP) is introduced. The CPCL lamellar structure without polymer is stabilized by the electrostatic interaction indicating that the fluctuations of the bilayer are strongly suppressed by the long-range electrostatic interaction [2,18]. The addition of polymer chains into the lamellar membranes induces a decrease of the smectic compressibility in the above four regimes, which is well described by the theoretical predictions [11]. Furthermore, when the electrostatic interaction is screened by salt, the addition of polymer brings a lamellar-lamellar phase separation [11,12]. Thus, the effective inter-lamellar interaction mediated by the presence of polymer chains is attractive.

On the other hand, if the guest component has a hard-core potential, the fluctuations of lamellar membranes might be strongly affected by the excluded-volume effect.

[a] e-mail: imai@phys.ocha.ac.jp

Ponsinet *et al.* [19,20] found that colloidal magnetic particles stabilizes the lamellar phase due to steric hindrance. From this standpoint, we systematically investigate the modulation of the inter-lamellar interactions between the fluctuating lamellar bilayers by the addition of guest components, namely, polymer chains having flexible entity or spherical colloidal particles having rigid entity. In this study we deal with the 3D D regime, thus the mean inter-lamellar distance is fairly larger than the size of the guest component and its volume fraction is quite low. We examine the non-ionic surfactant lamellar system, where the inter-lamellar interactions are governed by the entropic repulsive interaction, *i.e.*, Helfrich interaction [4]. The changes of the statical and dynamical structure of fluctuating lamellar bilayers induced by the guest components were measured by small-angle X-ray scattering (SAXS), small-angle neutron scattering (SANS) and neutron spin echo (NSE) techniques. From the SAXS, SANS and NSE profiles we can extract the elastic properties of the lamellar structure, that is the bending modulus and the layer compression modulus [2,3,21,22]. Especially, the behavior of the layer compression modulus is examined in terms of the modulation of the inter-lamellar interaction potential by the addition of the guest components.

2 Experimental section

We investigate ternary mixtures of water, $C_{12}E_5$ plus polymer or spherical colloid particle. The non-ionic surfactant $C_{12}E_5$ (purity $> 98\%$) was purchased from Nikko Chemicals Inc., and used without further purification. The phase behavior of the $C_{12}E_5$/water system is well characterized and we can control the inter-lamellar distance by a simple dilution law [23]. First, we investigated the phase behavior of the water, $C_{12}E_5$ and polyethylene oxide (PEO) mixture system. This polymer is non-ionic and easily soluble in the lamellar phase of the $C_{12}E_5$/water system. The PEO sample has molecular weight $\sim$ 70000, which corresponds to a radius of gyration, R_g, of 128 Å [24], and was obtained from Wako Pure Chemical Industries, Ltd. The volume fraction of PEO, Φ_{PEO}, was calculated using the following densities: 1.00 g cm^{-3} (H_2O); 1.104 g cm^{-3} (D_2O); 0.967 g cm^{-3} ($C_{12}E_5$); 1.21 g cm^{-3} (PEO). The phase behavior of the water, $C_{12}E_5$ and colloidal-particle system was investigated using a polystyrene latex having diameter 200 Å (±80 Å), which was obtained from Magsphere Inc. The polystyrene latex has surface charge $\sim 0.1e/\mathrm{nm}^2$, which is high enough to prevent it from aggregation. The ionic strength I of the colloidal suspension is expressed by the relation $I(\mathrm{mM}) = 24\rho_{col}(\mathrm{wt}\%)$, where ρ_{col} is the weight fraction of colloidal particles. Thus the colloidal suspension with $\rho_{col} = 0.01\%$ has an ionic strength of 0.24 mM. We confirmed that the scattering profile of the lamellar structure was not affected by the presence of the small amount of the ionic species. The volume fraction of the polystyrene colloidal particle Φ_{col} was calculated using a density of 1.05 g/cm^3.

The ternary-mixture samples for the scattering measurements were prepared by the following procedure. The surfactant and water mixtures ($C_{12}E_5/D_2O$ for SANS and $C_{12}E_5/H_2O$ for SAXS) were homogenized and then the guest components were added to the surfactant solution at room temperature (isotropic micelle phase). The sample was transferred to a cell for scattering measurements and then annealed at a measurement temperature of 70 °C (lamellar phase). The standard thickness of the sample cell for SANS measurements was 4.0 mm or above. In the standard sample cells, the lamellar phase prefers polycrystalline arrangements. During the scattering measurements, we regulated the temperature within ±0.01 °C.

SAXS measurements were performed using the BL-15A instrument at the photon factory (PF) in the high-energy accelerator research organization (KEK) [25]. In this experiment we used a 1.5 Å wavelength X-ray beam having $0.8 \times 0.8\,\mathrm{mm}^2$ square cross-section. The scattered beam was recorded using the CCD area detector covering a scattering vector q ($q = 4\pi \sin\theta/\lambda$) range from 0.03 to 0.33 Å^{-1}. The obtained scattering patterns were corrected for the non-uniformity, image distortion and background scattering.

SANS measurements were carried out using the SANS-U instrument of the Institute of Solid State Physics, University of Tokyo at the JRR3-M reactor of the Japan Atomic Energy Research Institute in Tokai [26]. In this experiment, we used a neutron beam having a wavelength (λ) of 7.0 Å with 10% resolution. The diameter of the irradiated neutron beam was 5 mm and the scattered neutrons were detected by a two-dimensional position-sensitive detector having $65 \times 65\,\mathrm{cm}^2$ (128×128 pixels) area. By changing the sample-to-detector distance, we covered the q range from 0.002 to 0.3 Å^{-1}. The obtained two-dimensional isotropic scattering patterns were corrected for background scattering and then circularly averaged to obtain one-dimensional scattering profiles.

The intermediate scattering functions of the samples were obtained using the NSE spectrometer at the C2-2 port of the JRR-3M reactor [27]. The incident neutron wavelength was 7.14 Å with 18% resolution, which covers a q range from 0.04 to 0.16 Å^{-1}. The Fourier time range of the spectrometer is $0.08 < t < 15$ ns. The obtained intermediate scattering function $S(q,t)$ was corrected using a resolution standard sample of Grafoil.

3 Results and discussion

In this section we describe the features of lamellar + guest systems in the following way. First, we show the difference in the phase behavior between the lamellar + polymer system and the lamellar + colloid-particle system. Before doing a detailed analysis for lamellar + guests systems, we examine the dominant interactions between the non-ionic surfactant membranes without guests using experimental results of SANS and NSE measurements. Then, the phase behavior of the lamellar + polymer system will be discussed based on Ligoure's model. A characteristic phase

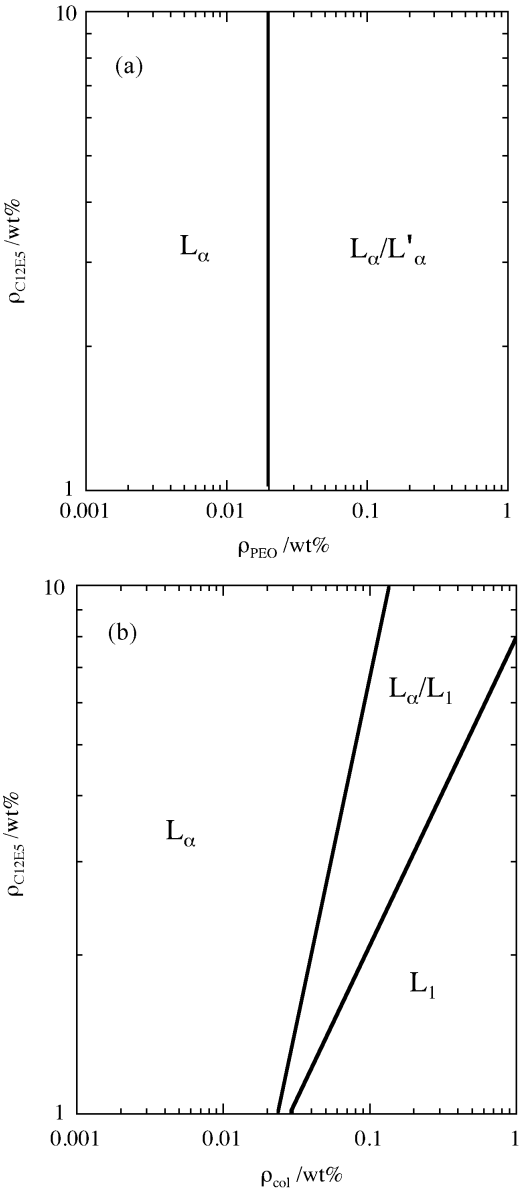

Fig. 1. Phase diagrams at $T = 57\,^\circ$C of the ternary $C_{12}E_5$/water/PEO system (a) and $C_{12}E_5$/water/colloidal-particle system (b). The vertical axis is the weight fraction of the surfactant $\rho_{C_{12}E_5}$ and the horizontal axis is the weight fraction of the guest components, PEO (ρ_{PEO}) (a) and colloidal particle (ρ_{col}) (b). L_α: lamellar phase, L_1: micelle phase, L_α/L'_α: lamellar and lamellar two-phase region having different spacing, and L_α/L_1: lamellar and micelle two-phase region.

behavior observed in the lamellar + colloidal-particle system will be investigated in terms of an entropical repulsive interaction model.

3.1 Phase behaviors of lamellar + polymer and lamellar + colloid-particle systems

First, we briefly compare phase behaviors of the lyotropic lamellar membrane + polymer system and lyotropic lamellar membrane + colloidal-particle system. Figure 1 shows the $\rho_{C_{12}E_5}$-ρ_{PEO} phase diagram and the $\rho_{C_{12}E_5}$-ρ_{col} phase diagram of the ternary system at $T = 57\,^\circ$C ($\rho_{C_{12}E_5}$: weight fraction of $C_{12}E_5$, ρ_{PEO}: weight fraction of PEO). We waited several weeks to examine the stability of the observed phases, because in the case of lamellar + guest component systems it took extremely long time to equilibrate the phases [11]. The addition of PEO chains into the lamellar phase brings the phase separation for $\rho_{PEO} > 0.02\,$wt%, which is presumably the coexistence of surfactant-rich lamellar phase and polymer-rich dilute lamellar phase [28]. This observation is consistent with the previous results [8,12]. The phase separation concentration was independent of the surfactant concentration. On the other hand, by the addition of spherical colloidal particles, the lamellar phase transformed to the micellar phase through the coexistence of lamellar and micellar phases. The phase transition concentration ρ_{col} increased with the increase of the surfactant concentration $\rho_{C_{12}E_5}$. The samples in the lamellar phase without the guest components are monophasic and slightly cloudy. By the addition of the colloidal particles, the samples became transparent and were a clear fluid in the L_1-phase, whereas by the addition of PEO the samples became cloudy.

The difference between the polymer chains and the colloidal particles becomes apparent by measuring SANS profiles. Figure 2 shows a series of SANS profiles as a function of (a) ρ_{PEO} and (b) ρ_{col} at constant $\Phi_{C_{12}E_5} = 0.045$. Unfortunately, there is no visible Bragg peak in the SANS profile of the $\Phi_{C_{12}E_5} = 0.045$ sample without guest species, because of the large membrane fluctuations. The membrane fluctuations cause the excess scattering observed in the low-q region [29]. In this case, we evaluate the lamellar repeat distance d from the following relationship in the literature [23]:

$$d = \frac{\delta}{\Phi_{C_{12}E_5}} \left(1 - \frac{k_B T}{4\pi\kappa_0} \ln \Phi_{C_{12}E_5}\right), \qquad (1)$$

where δ is the thickness of the membrane and κ_0 is the bare elastic bending modulus of a single membrane. Using $\delta = 30$ Å and $\kappa_0 = 1.3 k_B T$, we obtained $d(\Phi_{C_{12}E_5} = 0.045) = 794$ Å. Thus, the size of the guest components is much smaller than the period, and we are in the 3D D region. By the addition of PEO chains, the scattering functions keep the initial profile until $\rho_{PEO} \sim 0.03\%$ and then the scattering intensity in the low-q region increases with increase of ρ_{PEO}, which is due to the phase separation. On the other hand, the addition of colloidal particles brings the sharpening of the first Bragg peak and even the emergence of the second harmonic as shown in Figure 2(b). Thus, the inter-lamellar interactions induced by the addition of the guest components strongly depend on the nature of the guest species.

3.2 Non-ionic surfactant lamellar membrane without guests

First, we examine the dominant inter-lamellar interaction of a non-ionic surfactant membrane. Generally, it is

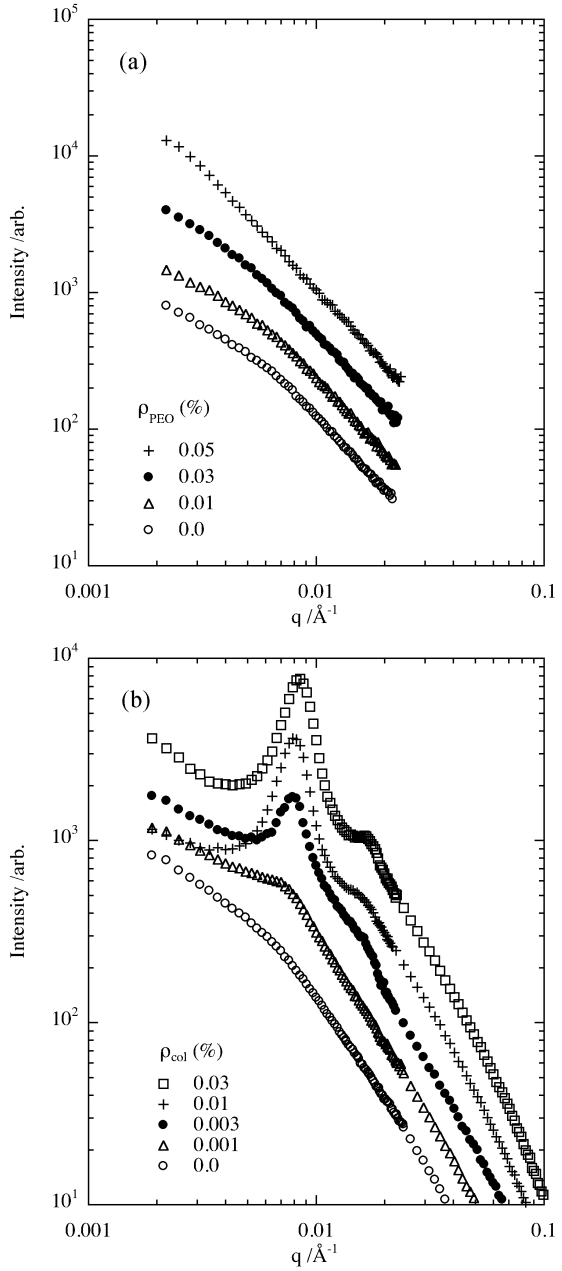

Fig. 2. SANS profiles of the lamellar phase confining guest components, PEO (a) and colloidal particle (b), at constant surfactant volume fraction $\Phi_{C_{12}E_5} = 0.045$ with varying the guest components fraction.

considered that the inter-lamellar interaction of the nonionic surfactant membrane system is governed by the Helfrich mechanism. For the Helfrich interaction [4], the potential energy is expressed by

$$F_{\mathrm{Hel}} = \frac{(k_{\mathrm{B}}T)^2}{32m\kappa\bar{d}^2}\,, \tag{2}$$

where m is the measure of the mean amplitude of thermal undulations of the membrane restricted by steric hindrance due to the adjacent bilayers, $\bar{d}$ is the average thickness of the water layer between two adjacent bilayers expressed by $\bar{d} = d - \delta$ (δ: bilayer thickness), k_{B} is Boltzmann's constant, and T is the temperature. Using the local displacements of the membrane $u(r)$ and $\bar{d}$, m is expressed by

$$\langle u^2(r)\rangle = m\bar{d}^2\,. \tag{3}$$

The expression of equation (2) is different from the usual expression for the Helfrich interaction with $m = 4/(3\pi^2)$, because the numerical prefactor is still under controversy [30]. Hereafter we use the prefactor $1/(32m)$ for the Helfrich interaction. When the inter-lamellar forces are dominated by the Helfrich interaction given by equation (2), we can expect to follow the simple geometrical expression [1]

$$\eta = \frac{2\pi}{\sqrt{3/m}}\left[1 - \frac{\delta}{d}\right]^2\,. \tag{4}$$

Here the Caillé parameter η is related to the elastic nature of the membrane by the following expression [31]:

$$\eta = \frac{q_0^2 k_{\mathrm{B}}T}{8\pi\sqrt{K\bar{B}}}\,, \tag{5}$$

where K is the bulk bending modulus having a relationship $K = \kappa/d$, $\bar{B}$ is the layer compression modulus, and q_0 is the position of the first Bragg singularity, $q_0 = 2\pi/d$. The Caillé parameter can be estimated from the SAXS or SANS profiles of the lamellar phase.

Figure 3 shows the SAXS profiles of the $C_{12}E_5$/water system as a function of $\Phi_{C_{12}E_5}$ at 70 °C (lamellar phase) in an $I(q)q^4$-q plot. In order to obtain the Caillé parameter, the scattering profiles were fitted by the model scattering function for the undulating lamellar structure proposed by Nallet *et al.* [3]:

$$I_{\mathrm{powd}}(q) \sim \frac{N_{\mathrm{l}}}{q^2}P(q)S(q)\,, \tag{6}$$

$$P(q) = \frac{4}{q^2}\{\Delta\rho_H[\sin[q(\delta_H+\delta_T)] - \sin(q\delta_T)] + \Delta\rho_T\sin(q\delta_T)\}^2\,, \tag{7}$$

$$S(q) = 1 + 2\sum_{n=1}^{N_{\mathrm{l}}-1}\left(1 - \frac{n}{N_{\mathrm{l}}}\right)\cos\left(\frac{qdn}{1+2\Delta q^2d^2\alpha(n)}\right) \times \exp\left[-\frac{2q_z^2d^2\alpha(n) + \Delta q^2d^2n^2}{2(1+2\Delta q^2d^2\alpha(n))}\right] \times \frac{1}{\sqrt{1+2\Delta q^2d^2\alpha(n)}}\,, \tag{8}$$

where N_{l} is the number of lamellar layers, Δq is the width of the resolution function assuming a Gaussian profile, and $\Delta\rho_H$ and $\Delta\rho_T$ are the contrast between the hydrophilic layer (thickness δ_H) and the solvent (H_2O), and between the hydrophobic part (thickness δ_T) and the solvent, respectively. In this model the correlation function for undulating lamellae $\alpha(n) = \langle(u_n - u_0)^2\rangle/2d^2$ in equation (8) is expressed by

$$\alpha(n) = \frac{\eta}{4d^2\pi^2}[\ln(\pi n) + \gamma]d^2 \tag{9}$$

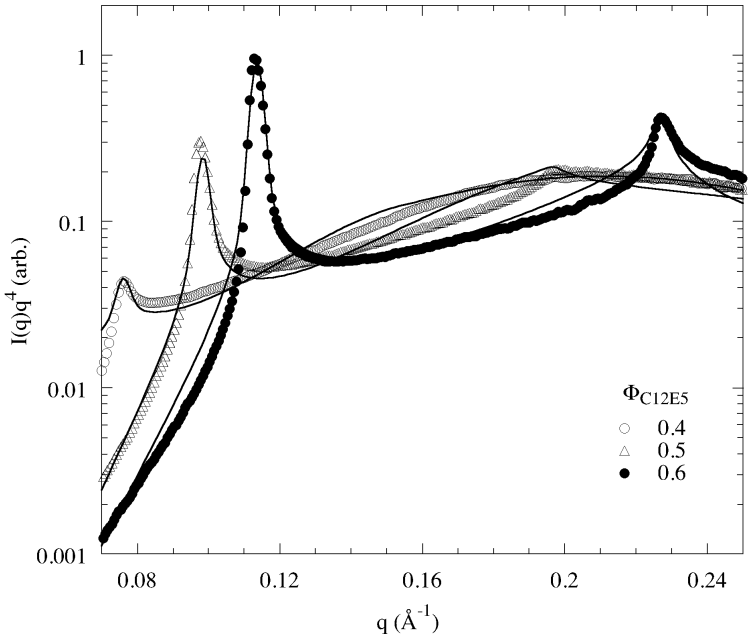

Fig. 3. SAXS profiles of the lamellar phase for the pure $C_{12}E_5$/water system as a function of $\Phi_{C_{12}E_5}$ in an $I(q)q^4$-*versus*-q plot. The solid lines are least-square fitting curves using the model scattering function proposed by Nallet *et al.*

with Euler's constant $\gamma = 0.5772$. The results of fitting are shown in Figure 3 by the solid lines. The experimentally obtained η is plotted against $(1-\delta/d)^2$ in Figure 4. Here we used $\delta = 30$ Å [23]. According to equation (4), this plot should give a straight line through the origin and its slope corresponds to the prefactor $2\pi/\sqrt{3/m}$. The expected value for the slope is 4/3 by the Helfrich prediction ($m = 4/(3\pi^2)$) [4], and $4\sqrt{2}/3$ by the computer simulations ($m = 8/(3\pi^2)$) [30]. The solid line in Figure 4 shows the best fit of experimental data with equation (4) and gives a slope of $1.85 \sim 4\sqrt{2}/3$, which corresponds to $m = 0.26 \sim 8/(3\pi^2)$. Hence we concluded that the inter-lamellar interaction of the lyotropic lamellar phase consisting of the non-ionic surfactant $C_{12}E_5$ is governed by the Helfrich interaction.

Next, we estimate the bending modulus κ from the intermediate scattering function $I(q,t)$ of a fluctuating membrane obtained by the NSE measurement [21,22]. Generally, the intermediate scattering function is expressed by

$$I(\boldsymbol{q},t) = N_{\mathrm{s}}^{-1}\sum_{i=1}^{N_{\mathrm{s}}}\sum_{j=1}^{N_{\mathrm{s}}}\langle\exp\{-i\boldsymbol{q}\boldsymbol{r}_i(0)\}\exp\{i\boldsymbol{q}\boldsymbol{r}_j(t)\}\rangle\,, \tag{10}$$

where N_{s} is the number of scattering particles. Zilman and Granek [21] derived the expression for the normalized intermediate scattering function of the fluctuating membranes:

$$\frac{I(q,t)}{I(q,0)} = \exp\{-(\Gamma_z t)^{2/3}\}\,, \tag{11}$$

$$\Gamma_z = D_z q^3\,, \tag{12}$$

$$D_z = 0.0056\gamma_\kappa (k_{\mathrm{B}}T)^{3/2}\kappa^{-1/2}\eta_\kappa^{-1}\,, \tag{13}$$

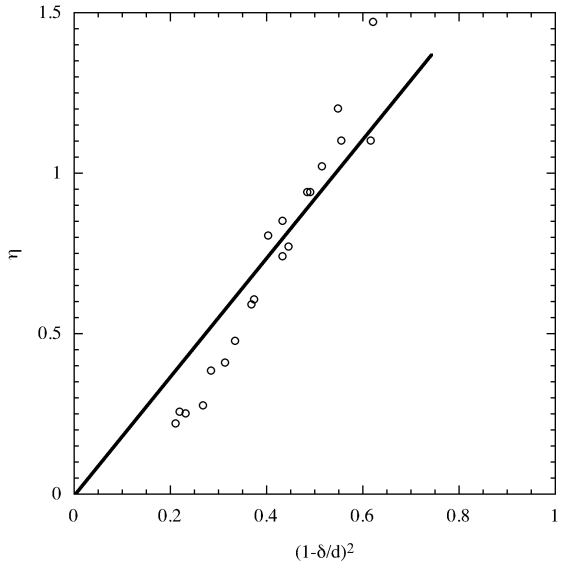

Fig. 4. The Caillé parameter η *versus* the $(1-\delta/d)^2$ plot for the pure $C_{12}E_5$/water system.

where η_κ is the viscosity of water. γ_κ is given by

$$\gamma_\kappa = 1 - 3\frac{\ln(q\xi)k_{\mathrm{B}}T}{4\pi\kappa}\,, \tag{14}$$

where ξ is the typical size of the mesoscopic structure of the system. Thus, we can obtain κ from the normalized intermediate scattering function. The normalized intermediate scattering functions for the $C_{12}E_5$/water system ($\Phi_{C_{12}E_5} = 0.045$) obtained from the NSE experiments are shown in Figure 5 with the fitting curves using the stretched exponential form of equation (11). The

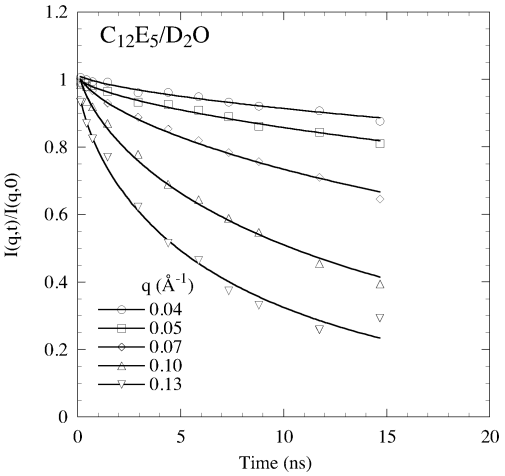

Fig. 5. Normalized intermediate scattering functions of the lamellar phase for the pure $C_{12}E_5$/water system at 57 °C ($\Phi_{C_{12}E_5} = 0.045$). The solid lines are least-square fitting curves using the Zilman-Granek theory.

relaxation rate Γ_z obtained by the fitting shows the power law of q^3 in agreement with the Zilman and Granek theory. However, it is still a controversy for the value of numerical parameters to evaluate the bending modulus from equations (11–14), because when the macroscopic viscosity of the solvent η_κ is used, one obtains a fairly large value of the bending modulus compared with the bending modulus estimated from other techniques. In order to fill up this gap, some adjustment techniques have been proposed [22,32,33]. A familiar technique for the adjustment is to use an effective viscosity $\eta_{\rm eff}$ instead of the macroscopic viscosity η_κ. The effective viscosity corrects the local dissipation at the interface between the membrane and the solvent, although the value of $\eta_{\rm eff}$ is determined by the phenomenological considerations. It is interesting to note that the intermediate scattering functions obtained from a dynamical light scattering (DLS) method give consistent bending moduli without the viscosity correction [34,35]. Then, we estimated κ of the standard lamellar sample ($C_{12}E_5/D_2O$: $\Phi_{C_{12}E_5} = 0.015$ at 57 °C) by the NSE and DLS measurements. The NSE and the DLS measurements gave values of $\kappa_{\rm NSE} = 9.05 k_{\rm B}T$ and $\kappa_{\rm DLS} = 2.01 k_{\rm B}T$, respectively, and the value of $\kappa_{\rm DLS}$ is close to the reported values for κ obtained from other methods [36]. From these experimental results, we estimated the value of $\eta_{\rm eff} = \sqrt{9.05/2.01} \cong 2.1\eta_\kappa$, which is slightly smaller than the value used in reference [22]. In this study, we used this effective viscosity to obtain κ from the NSE measurements. For the pure $C_{12}E_5/D_2O$ lamellar sample of $\Phi_{C_{12}E_5} = 0.045$, we obtained $\kappa = 3.1 k_{\rm B}T$ from $\kappa_{\rm NSE} = 14 k_{\rm B}T$ (at $\Phi_{C_{12}E_5} = 0.045$) using $\xi = 794$ Å ($\sim d$) [37].

When the inter-lamellar interaction is governed by the Helfrich mechanism, the layer compression modulus is expressed by [4]

$$\bar{B}^{\rm Hel} = \frac{3(k_{\rm B}T)^2}{16 m \kappa \bar{d}^4} d, \tag{15}$$

with $m = 0.26$ $\kappa = 3.1 k_{\rm B}T$, $d = 794$ Å and $\delta = 30$ Å, the evaluated value of the compression modulus for the pure $C_{12}E_5$/water ($\Phi_{C_{12}E_5} = 0.045$) system was $\bar{B}^{\rm Hel} \sim 25\,{\rm dyn/cm^2}$.

3.3 Lamellar + polymer system

Here we discuss the observed polymer-induced phase separation using the lamellar-lamellar phase separation model proposed by Ligoure *et al.* [11,15]. They found that the addition of the polymer into the smectic bilayer decreases the inter-lamellar repulsive force and finally brings the lamellar-lamellar phase separation when the layer compression modulus vanishes ($\bar{B} = 0$). In what follows, we briefly show an explanation for the observed phase behavior of the polymer-containing lamellar system based on Ligoure's scenario. In the case of the 3D D confinement system, the additional inter-lamellar interaction energy per unit bilayer area due to the polymer confinement is given by

$$F_{\rm pol} \cong \frac{k_{\rm B}T}{a^3} \bar{d} \frac{\bar{\Phi}_{\rm eff}}{N} \log(\bar{\Phi}_{\rm eff}), \tag{16}$$

where a is the monomer length of the polymer, and N is the degree of polymerization. The effective volume fraction of polymers in the inter-lamellar water layer $\bar{\Phi}_{\rm eff}$ is corrected due to the depletion zone covering the interface between water and bilayer,

$$\bar{\Phi}_{\rm eff} = \Phi_{\rm PEO} \frac{\bar{d}}{\bar{d} - 2R_{\rm g}}, \tag{17}$$

where $R_{\rm g}$ is the radius of gyration of a polymer coil. This additional potential energy modifies the compression modulus of the lamellar phase which is accessible from the scattering experiments. In the case of the lamellar phase containing guest components, the layer compression modulus is expressed by [38]

$$\bar{B}_\mu = d \left\{ \frac{\partial^2 F}{\partial \bar{d}^2} - \frac{\left[\frac{1}{\bar{d}} \frac{\partial F}{\partial \bar{\Phi}_{\rm g}} - \frac{\partial^2 F}{\partial \bar{\Phi}_{\rm g} \partial \bar{d}} \right]^2}{\frac{\partial^2 F}{\partial \bar{\Phi}_{\rm g}^2}} \right\}, \tag{18}$$

where $\bar{\Phi}_{\rm g}$ is the volume fraction of the guest component in the water layer. Using this expression, the contribution of the confined polymer to the layer compression modulus is given by [11]

$$\bar{B}_\mu^{\rm pol} = -\frac{4 k_{\rm B}T R_{\rm g}^2 d \bar{\Phi}}{a^3 N \bar{d}^3} \left(1 + \log \left[\frac{\bar{d}\bar{\Phi}}{\bar{d} - 2R_{\rm g}} \right] \right)^2. \tag{19}$$

Here we assume that the total inter-lamellar interaction for the lamellar membrane + polymer system is expressed by the sum of the two terms [11,15]:

$$F_{\rm total} = F_{\rm pol} + F_{\rm Hel} \tag{20}$$

and the total layer compressibility is given by

$$\bar{B}_{\rm pol}^{\rm total} = \bar{B}_\mu^{\rm pol} + \bar{B}^{\rm Hel}. \tag{21}$$

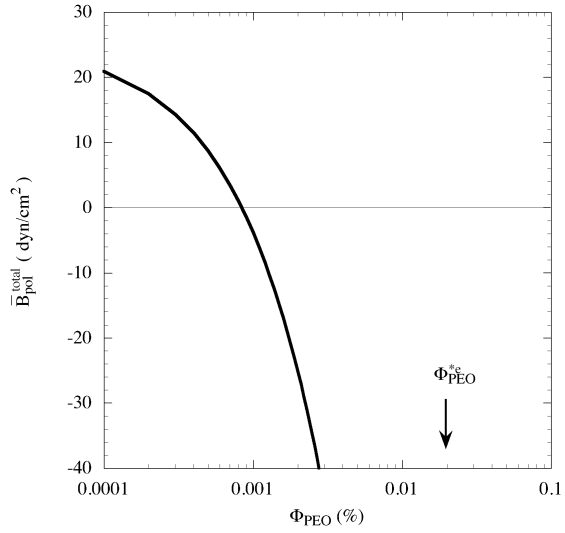

Fig. 6. Variation of the theoretical total layer compression modulus $\bar{B}^{\rm total}_{\rm pol}$ for the lamellar + PEO system as a function of $\Phi_{\rm PEO}$. The experimentally observed phase separation concentration $\Phi^{*\rm e}_{\rm PEO}$ is indicated by an arrow.

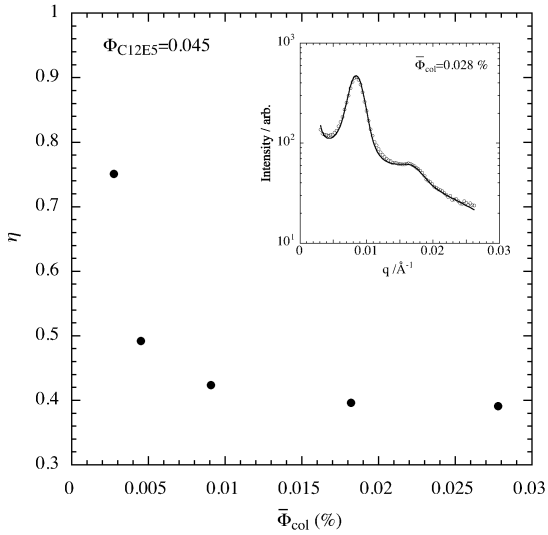

Fig. 7. Variation of the Caillé parameter η of the lamellar + colloid-particle system as a function of $\bar{\Phi}_{\rm col}$ at $\Phi_{\rm C_{12}E_5} = 0.045$. Inset: scattering profile for the lamellar + colloid-particle system ($\Phi_{\rm C_{12}E_5} = 0.045$ and $\bar{\Phi}_{\rm col} = 0.028\%$) with the fitting result (solid line) using equations (6–8).

It is important to note that the polymer contribution $\bar{B}^{\rm pol}_{\mu}$ is negative and induces destabilization of the lamellar phase. Experimentally, Ligoure *et al.* reported that by the addition of polymer in the lamellar system, the lamellar phase is destabilized by the additional attractive inter-lamellar interaction and finally undergoes a lamellar-lamellar phase separation at $\bar{B}^{\rm total}_{\rm pol} = \bar{B}^{\rm pol}_{\mu} + \bar{B}^{\rm Hel} = 0$. The value of $\bar{B}^{\rm pol}_{\mu}$ can be estimated by equation (19) using the statistic chain parameters a and N. For PEO chain, we determined the values of a and N from the experimental relationship

$$R_{\rm g}(\text{Å}) = 0.1078 \times M^{0.635}_{\rm PEO}\,, \tag{22}$$

where $M_{\rm PEO}$ is the molecular weight of PEO. The calculated values a and N for the PEO chain with $M_{\rm PEO} = 70000$ were $a = 5.6$ Å [24] and $N = 1070$. Using these values we obtained the $\bar{B}^{\rm pol}_{\mu}$ as a function of $\Phi_{\rm PEO}$:

$$\bar{B}^{\rm pol}_{\mu}\,({\rm dyn/cm^2}) = -2.85 \times 10^4 \Phi_{\rm PEO}(1 + \log[1.47\Phi_{\rm PEO}])^2. \tag{23}$$

In Figure 6 we plotted $\bar{B}^{\rm total}_{\rm pol} = \bar{B}^{\rm pol}_{\mu} + \bar{B}^{\rm Hel}$ as a function of $\Phi_{\rm PEO}$. Figure 6 shows that the $\bar{B}^{\rm total}_{\rm pol}$ decreases with increase of $\Phi_{\rm PEO}$ and crosses zero at $\Phi^{*\rm t}_{\rm PEO} \sim 0.001\%$, where the phase separation starts. Ligoure's model explain the phase separation behavior only qualitatively but quantitatively there is a large difference between the theoretical prediction and the experimental data $\Phi^{*\rm e}_{\rm PEO} \sim 0.02\%$. The discrepancy between theoretical prediction and experimental result may be originated from the ambiguity of the estimation of κ or $\bar{B}^{\rm Hel}$.

3.4 Lamellar + colloid-particle system

In the case of the non-ionic surfactant/water and colloidal-particle mixture system, the phase behavior is completely different from the non-ionic surfactant/water and polymer mixture system. The addition of colloidal particles brings the sharpening of the first Bragg peak and the emergence of the second harmonic as shown in Figure 2(b). This result is consistent with the behavior of the lamellar + colloidal-magnetic-particle system [19,20]. Here we consider the dominant inter-lamellar interaction in the presence of the spherical colloidal particles. In order to examine the inter-lamellar interaction, the scattering profiles for the $C_{12}E_5$ + colloidal-particle/water system were fitted using the scattering function proposed by Nallet *et al.*, equations (6–8). The variation of the obtained η as a function of $\bar{\Phi}_{\rm col}$ at $\Phi_{\rm C_{12}E_5} = 0.045$ is plotted in Figure 7. For reference, we display a typical fitting result of the scattering profile for the system ($\Phi_{\rm C_{12}E_5} = 0.045$ and $\bar{\Phi}_{\rm col} = 0.028\%$) in the figure. The Caillé parameter η decreases sharply as $\Phi_{\rm col}$ increases, until it reaches a plateau value of $\eta \sim 0.4$. Thus, the addition of hard-sphere colloidal particles brings restriction of undulation fluctuations of lamellar membranes at extremely low volume fraction of the colloid particle. An interesting feature of the inter-lamellar interaction induced by the confinement of colloidal particles is the dependence of the Caillé parameter η on the lamellar spacing d as shown in Figure 8. When the inter-lamellar distance is governed by the Helfrich interaction, η obeys the simple geometrical expression $\eta = 1.85(1 - \delta/d)^2$. Thus, η determined by the Helfrich interaction increases with increase of d as shown by the solid line in Figure 8. On the contrary, in the presence of colloidal particles, η decreases monotonically with increase of d. Interestingly, the restriction of membrane fluctuations is remarkable in the dilute lamellar region.

In order to elucidate this characteristic inter-lamellar interaction induced by the addition of colloidal particle,

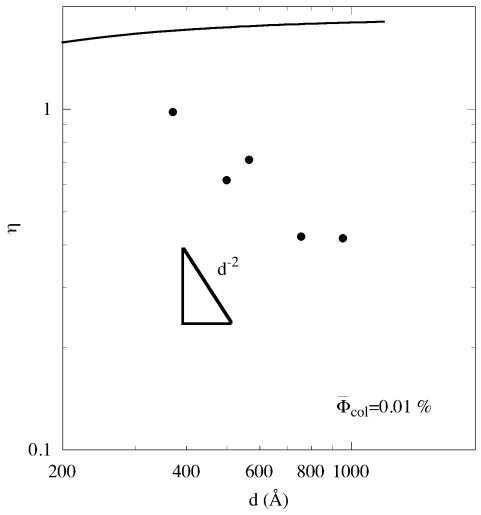

Fig. 8. Variation of the Caillé parameter η of the lamellar + colloid-particle system as a function of d at $\bar{\Phi}_{\rm col} = 0.01\%$. The solid line is the prediction of the Helfrich model.

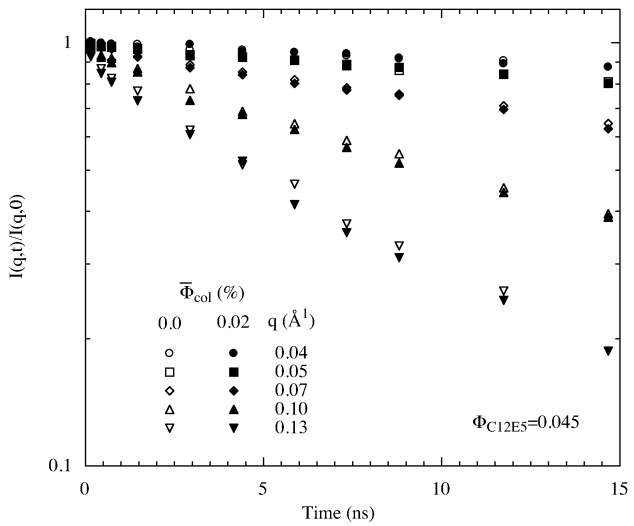

Fig. 9. Normalized intermediate scattering functions of the lamellar system and the lamellar + colloidal-particle system at $\Phi_{\rm C_{12}E_5} = 0.045$.

we estimated the layer compression modulus $\bar{B}$. For this purpose we obtained the bending modulus of the membrane of the $C_{12}E_5$/water + colloidal-particle systems by the NSE experiments. The comparison of intermediate scattering functions between lamellar system and lamellar + colloidal-particle system is shown in Figure 9. The intermediate scattering functions were independent of the addition of the colloidal particles and obeyed the stretched exponential low of equation (11). The Zilman-Granek analysis of the observed intermediated scattering functions gives the bending modulus κ. The value of κ was independent of $\Phi_{\rm col}$ in the range $0 < \Phi_{\rm col} < 0.02\%$ and kept the original value $\sim 3k_{\rm B}T$. Using the values of η and κ, we obtained the layer compression modulus $\bar{B}$ as a function of $\Phi_{\rm col}$ (Fig. 10). The layer compression modulus $\bar{B}$ increases

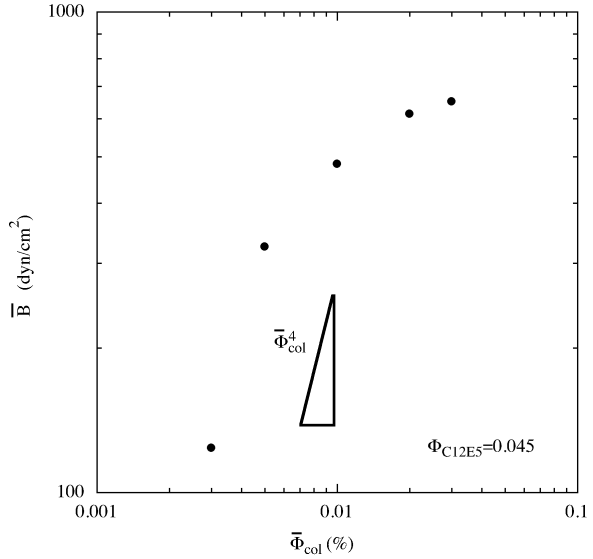

Fig. 10. Variation of the experimentally obtained layer compression modulus $\bar{B}$ for the lamellar + colloid-particle system as a function of $\bar{\Phi}_{\rm col}$ at $\Phi_{\rm C_{12}E_5} = 0.045$. The theoretical prediction $\bar{B}_{\mu}^{\rm col} \sim \bar{\Phi}_{\rm col}^4$ is indicated in the figure.

from $\sim 25\,{\rm dyn/cm^2}$ ($\Phi_{\rm col} = 0$) with increase of $\Phi_{\rm col}$ and reaches an equilibrium value ~ 600 dyn/cm^2. Thus the addition of hard-sphere colloids brings strong repulsive force between adjacent lamellar layers and this effect is remarkable at low concentrations of the non-ionic surfactant. This observation is hardly explained by the previous model for the 3D D region, because in this model the addition of guest components necessarily brings negative contribution to the layer compression modulus as shown in equation (19).

In order to explain the observed experimental results, we took into account the suppression of membrane fluctuations due to the excluded-volume effect of the colloidal particles, which gives the entropic repulsive inter-lamella interaction. Here we derive the expression of the steric repulsive interaction potential. First, we introduce a dimensionless surface coverage parameter defined by

$$\chi = \pi R^2 n^{\rm col} = \pi R^2 \frac{3\bar{\Phi}_{\rm col} d}{4\pi R^3} = \frac{3\bar{\Phi}_{\rm col} d}{4R}\,, \qquad (24)$$

where $n^{\rm col}$ is the number of colloidal particles per unit bilayer area. We assume that the restriction of the membrane fluctuations is expressed by a function of the surface coverage χ, that is

$$|u(r)| \leqslant \bar{d} f(\chi)\,. \qquad (25)$$

The function $f(\chi)$ has the following features: i) $f(\chi) \to 1$ for $\chi \to 0$, and ii) $f(\chi) \to 0$ for $\chi \to \infty$. In order to satisfy these conditions, we adopted the function given by

$$f(\chi) = \tanh^2(1/\alpha\chi)\,, \qquad (26)$$

where α is a coefficient to correct effective surface coverage. Using this function, the restriction of the membrane

fluctuations are expressed by

$$\langle u^2(r)\rangle = m_{\rm c}\bar{d}^2 \tanh^4\left(\frac{4R}{3\alpha\bar{\Phi}_{\rm col}d}\right), \qquad (27)$$

where the factor $m_{\rm c}$ must be smaller than unity. Following the Helfrich formalism [4], the free energy of the steric interaction per unit area of a membrane is given by

$$F_{\rm col} = \frac{(k_{\rm B}T)^2}{32m_{\rm c}\kappa}\frac{1}{\bar{d}^2\tanh^4(\frac{4R}{3\alpha\bar{\Phi}_{\rm col}d})}. \qquad (28)$$

For $\alpha\chi \ll 1$, $\tanh^4(\frac{4R}{3\alpha\bar{\Phi}_{\rm col}d})$ approaches unity. Then equation (28) agrees with the expression for the usual Helfrich interaction free energy, equation (2). On the other hand, in the high surface coverage region $\alpha\chi \gg 1$, the free energy is expressed by

$$F_{\rm col} = \frac{(k_{\rm B}T)^2}{32m_{\rm c}\kappa}\left(\frac{3\alpha\bar{\Phi}_{\rm col}}{4R}\right)^4\frac{d^4}{\bar{d}^2} \qquad \text{for } \alpha\chi \gg 1. \qquad (29)$$

Using this free-energy expression and equation (18), the layer compression modulus is given by

$$\bar{B}_\mu^{\rm col} = \frac{(k_{\rm B}T)^2}{3m_{\rm c}\kappa}\left(\frac{3\alpha\bar{\Phi}_{\rm col}}{16R_{\rm col}}\right)^4\frac{d^5}{\bar{d}^4} \qquad \text{for } \alpha\chi \gg 1. \qquad (30)$$

In Figure 10 we compared the theoretical prediction $\bar{B}_\mu^{\rm col}$ with the experimentally obtained $\bar{\Phi}_{\rm col}$-dependence of $\bar{B}$. The steep increase of $\bar{B}$ with increase of $\bar{\Phi}_{\rm col}$ is well described by equation (30). Here we assume that the coefficient α takes a large value ($> 10^3$). This large α means that the presence of one colloidal particle affects fluctuations of a large membrane area. The experimentally obtained $\bar{B}$ deviates from the theoretical prediction and levels off at high $\bar{\Phi}_{\rm col}$. This deviation may be originated from the fact that the form of $f(\chi)$ given by equations (24) and (26) is not valid at high $\bar{\Phi}_{\rm col}$. Thus, the layer compression modulus is independent of $\bar{\Phi}_{\rm col}$ at $\chi \gg 1$, because the $\bar{\Phi}_{\rm col}$ reaches a saturated value. Using equation (30), the Caillé parameter of this system is expressed by

$$\eta^{\rm col} = \frac{\pi\sqrt{3m_{\rm c}}}{2\Phi_{\rm col}^2}\left(\frac{16R}{3\alpha}\right)^2\left(\frac{\bar{d}}{d}\right)^2\frac{1}{d^2} \qquad \text{for } \alpha\chi \gg 1. \qquad (31)$$

In Figure 8 we compared this theoretical prediction with the experimental results. Taking into account $\bar{d}/d \cong 1$, the characteristic d-dependence of η is well described by equation (31). Thus, the colloidal particles introduced between lamellar membranes restrict the membrane fluctuations due to the hard-sphere nature, which brings steric repulsive inter-lamellar interactions.

4 Conclusions

The inter-lamellar interaction induced by the addition of the guests depends on the rigidity of the added materials. The addition of neutral polymer into the lamellar phase induces an attractive inter-lamellar interaction and finally destabilizes the single lamellar phase. This behavior is qualitatively described by a free-energy model for polymer-containing lyotropic lamellar phases developed by Ligoure *et al.* On the other hand, the spherical colloidal particles confined between the flexible lamellar membranes suppress lamellar fluctuations and bring a repulsive inter-lamellar interaction. The behavior of the layer compression modulus of the lamellar membrane containing colloidal particles is well described by the entropical repulsive inter-lamellar interaction driven by steric hindrance. The difference between polymer and colloid particle is probably attributed to the fact that the polymer chains do not suppress the membrane fluctuations due to their large internal degrees of freedom.

This work is supported by a Grant-in-Aid for Scientific Research (B) (No. 15340138) and (C) (No. 15540395) from the Ministry of Education, Science, Sports and Culture of Japan. The SANS and NSE experiments were done under the approval of the Neutron Scattering Program Advisory Committee (Proposal No. 3541).

References

1. D. Roux, C.R. Safinya, J. Phys. (Paris) **49**, 307 (1988).
2. D. Roux, F. Nallet, E. Freyssingeas, G. Porte, P. Bassereau, M. Skouri, J. Marignan, Europhys. Lett. **17**, 575 (1992).
3. F. Nallet, R. Laversanne, D. Roux, J. Phys. II **3**, 487 (1993).
4. W. Helfrich, Z. Naturforsch. A **33**, 305 (1978).
5. M. Daoud, P.G. de Gennes, J. Phys. (Paris) **38**, 85 (1977).
6. J.T. Brooks, C.M. Marques, M.E. Cates, J. Phys. II **1**, 673 (1991).
7. J.T. Brooks, M.E. Cates, J. Chem. Phys. **99**, 5467 (1993).
8. C. Ligoure, G. Bouglet, G. Porte, Phys. Rev. Lett. **71**, 3600 (1993).
9. M.-F. Ficheux, A.-M. Bellocq, F. Nallet, J. Phys. II **5**, 823 (1995).
10. E.Z. Radlinska, T. Gulik-Krzywicki, F. Lafuma, D. Langevin, W. Urbach, C.E. Williams, R. Ober, Phys. Rev. Lett. **74**, 4237 (1995).
11. C. Ligoure, G. Bouglet, G. Porte, O. Diat, J. Phys. II **7**, 473 (1997).
12. L. Porcar, C. Ligoure, J. Marignan, J. Phys. II **7**, 493 (1997).
13. G. Bouglet, C. Ligoure, A.-M. Bellocq, E. Dufoure, G. Mosser, Phys. Rev. E **57**, 834 (1998).
14. Y. Yang, R. Prudhomme, K.M. McGrath, P. Richetti, C.M. Marques, Phys. Rev. Lett. **80**, 2729 (1998).
15. G. Bouglet, C. Ligoure, Eur. Phys. J. B **9**, 137 (1999).
16. F. Castro-Roman, G. Porte, C. Ligoure, Phys. Rev. Lett. **82**, 109 (1999).
17. M.-F. Ficheux, A.-M. Bellocq, F. Nallet, Eur. Phys. J. E **4**, 315 (2001).
18. P. Pincus, J.-F. Joanny, D. Andelman, Europhys. Lett. **11**, 763 (1990).
19. V. Ponsinet, P. Fabre, M. Veyssie, L. Auvray, J. Phys. II **3**, 1021 (1993).
20. V. Ponsient, P. Fabre, J. Phys. II **6**, 955 (1996).

21. A.G. Zilman, R. Granek, Phys. Rev. Lett. **77**, 4788 (1996).
22. S. Komura, T. Takeda, Y. Kawabata, S.K. Ghosh, H. Seto, M. Nagao, Phys. Rev. E **63**, 041402 (2001).
23. R. Strey, R. Schomäcker, D. Roux, F. Nallet, U. Olsson, J. Chem. Soc. Faraday Trans. **86**, 2253 (1990).
24. F. Castro-Roman, C. Ligoure, Europhys. Lett. **53**, 483 (2001).
25. Y. Amemiya, K. Wakabayashi, T. Hamanaka, T. Wakabayashi, T. Matsusita, H. Hashizume, Nucl. Instrum. Methods **208**, 471 (1983).
26. Y. Ito, M. Imai, S. Takahashi, Physica B **213&214**, 889 (1995).
27. T. Takeda, S. Komura, H. Seto, M. Nagai, H. Kobayashi, E. Yokoi, C.N.E. Zeyen, T. Ebisawa, S. Tasaki, Y. Ito, S. Takahashi, H. Yoshizawa, Nucl. Instrum. Methods Phys. Res. A **364**, 186 (1995).
28. We confirmed the lamellar-lamellar phase separation induced by the addition of PEO using the slightly high surfactant concentration sample ($\rho_{C_{12}E_5} \sim 20\%$), because the dilute samples do not have definite Bragg peaks.
29. G. Porte, J. Marignan, P. Bassereau, R. May, Europhys. Lett. **7**, 713 (1988).
30. R.R. Netz, R. Lipowsky, Europhys. Lett., **29**, 345 (1995).
31. A. Caillé, C.R. Acad. Sci. Ser. B **247**, 891 (1972).
32. B. Farago, M. Monkenbusch, K.D. Goecking, D. Richter, J.S. Haung, Physica B, **213&214**, 712 (1995).
33. M. Mihailescu, M. Monkenbusch, H. Endo, J. Allgaier, G. Gompper, J. Stellbrink, D. Richter, B. Jakobs, T. Sottmann, B. Farago, J. Chem. Phys. **115**, 9563 (2001).
34. E. Freyssingeas, D. Roux, F. Nallet, J. Phys. II **7**, 913 (1997).
35. Y. Kimura, J. Oizumi, R. Hayakawa, Mol. Cryst. Liq. Cryst. **332**, 559 (1999).
36. J. Oizumi, Y. Kimura, K. Ito, R. Hayakawa, Mol. Cryst. Liq. Cryst. **303**, 63 (1997).
37. T. Hellweg, Curr. Opin. Colloid Interface Sci. **7**, 50 (2002).
38. F. Nallet, D. Roux, C. Quilliet, P. Fabre, S.T. Milner, J. Phys. II **4**, 1477 (1994).